Valley Networks and the Record of Glaciation on Ancient Mars

A. Grau Galofre[1,2*], K.X. Whipple[1], P.R. Christensen[1], S.J. Conway[2]

[1]School of Earth and Space Exploration, Arizona State University, Tempe (AZ), United States
[2]Laboratorie du Planétologie et Géosciences/ CNRS UMR6112, Nantes Université, Nantes, France

Key Points:

- Glacial hydrology feedback dynamics can explain the lack of glacial sliding on the Martian geological record.
- Subglacial water drainage develops faster, and is more resilient under lower Martian gravity.
- The fingerprints of Martian wet-based glaciation are predicted to be channels and eskers.

*Now at the Laboratorie du Planétologie et Géosciences

Corresponding author: Anna Grau Galofre, `anna.graugalofre@univ-nantes.fr`

Abstract

The lack of evidence for large-scale glacial landscapes on Mars has led to the belief that ancient glaciations had to be frozen to the ground. Here we propose that the fingerprints of Martian wet-based glaciation should be the remnants of the ice sheet drainage system instead of landforms generally associated with terrestrial ice sheets. We use the terrestrial glacial hydrology framework to interrogate how the Martian surface gravity affects glacial hydrology, ice sliding, and glacial erosion. Taking as reference the ancient southern circumpolar ice sheet that deposited the Dorsa Argentea formation, we compare the theoretical behavior of identical ice sheets on Mars and Earth and show that, whereas on Earth glacial drainage is predominantly inefficient, enhancing ice sliding and erosion, on Mars the lower gravity favors the formation of efficient subglacial drainage. The apparent lack of large-scale glacial fingerprints on Mars, such as drumlins or lineations, is to be expected.

Plain Language Summary

Water accumulates under ice masses, including glaciers and ice sheets, lubricating the base of the ice and accelerating ice motion. On Earth, this glacial motion has produced scoured landscapes in northern Europe and north America. Mars lacks such large-scale glacial erosion even in areas with other signs of widespread glaciation. This paper uses the existing framework describing the physical interactions of water and ice, and how they affect ice motion, to show that a lack of landforms recording glacial erosion is expected even if glaciation were widespread on Mars.

1 Introduction

Large-scale continental glaciation is responsible for some of the most arresting landscapes on Earth. The retreat of Quaternary ice sheets revealed scoured landscapes sculpted by sliding ice masses, driven by the presence of basal water (wet-based glaciation). These glacial landscapes are distinctive, and include areal linear scouring at different scales, depositional and deformational landforms such as moraines and drumlins, and features associated with basal meltwater drainage, such as eskers, subglacial channels, and tunnel valleys.

Mars has had a significant cryosphere throughout history, including polar caps, glacial bodies, and ground ice (e.g., Kargel & Strom, 1992; Byrne, 2009; Carr & Head, 2015). However, the dearth of glacially scoured landscapes, which are typically associated with glacial sliding on Earth, has largely dissuaded researchers from considering widespread wet-based glaciation on Mars (e.g., A. Howard, 1981; Kargel et al., 1995; Bernhardt et al., 2013; Fastook & Head, 2015; Wordsworth, 2016). Martian ice masses are interpreted to have been fundamentally cold-based throughout history, with little erosional action (e.g., A. S. Dyke, 1993; Wordsworth, 2016; Alley et al., 2019).

This reasoning has two limitations. First, multiple landscapes on Mars contain evidence of glaciation. Those include the Dorsa Argentea formation (e.g., Fastook et al., 2012; Scanlon et al., 2018; Butcher et al., 2016), eskers in the mid-latitudes (e.g., Gallagher & Balme, 2015; Butcher et al., 2017, 2020), and possibly inside the Argyre and Hellas basins (e.g., Kargel & Strom, 1992; Bernhardt et al., 2013, 2019). The presence of eskers indicates that wet-based glaciation occurred (e.g., Fastook et al., 2012; Butcher et al., 2016; Boulton et al., 2009; Storrar et al., 2014), despite the absence of landforms associated with glacial sliding. Second, erosion by surface water flows points at warmer conditions on early Mars (>3.5 Gyr BP) (e.g., Craddock & Howard, 2002; A. D. Howard et al., 2005; Hynek et al., 2010) than at present, when surface ice deposits are too cold to melt or flow significantly (e.g., Fastook et al., 2008; Cuffey & Paterson, 2010; Nye et al., 2000; Hubbard et al., 2014). As the planet cooled and ice masses started to appear, a transitional period in which glaciers had some degree of basal melting is to be expected (e.g., Cuffey & Paterson, 2010; Wordsworth, 2016).

Here, we show quantitatively that the lower surface gravity on Mars should alter the behavior of wet-based ice masses by modifying the subglacial drainage system, making efficient, channelized drainage beneath Martian ice both more likely to form and more resilient to closure. Using as an example the case of the ancient southern circumpolar ice sheet (e.g., Fastook et al., 2012; Scanlon et al., 2018) we demonstrate that the expected fingerprint of wet-based Martian ice sheets is networks of subglacial channels and eskers, consistent with the occurrence of valley networks and inverted ridges found on the Martian highlands (Grau Galofre, Osinski, et al., 2020).

1.1 Glacial sliding and glacial erosion

According to the existing theory of terrestrial glacial motion and hydrology, creep deformation and basal sliding drive the motion of ice (e.g., Cuffey & Paterson, 2010). Creep deformation is the deformation of ice in response to stress, and is strongly dependent on temperature (e.g., Cuffey & Paterson, 2010; Glen, 1958). Basal sliding occurs when ice slips over the substrate, lubricated by the presence of pressurized basal water (e.g., Cuffey & Paterson, 2010; Schoof, 2005, 2010; Gagliardini et al., 2007). Whereas sliding dominates glacial erosion, the erosional role of creep deformation is believed to be less important (e.g., A. S. Dyke, 1993; Alley et al., 2019).

Water accumulated beneath ice (subglacial) is at a pressure P_w generally differing from ice overburden pressure P_i. This difference defines the effective pressure $N = P_i - P_w$, corresponding to the ice normal stress. If the basal water accumulation rate is faster than the drainage rate, P_w increases and effective pressure N decreases. N nears zero ($N \to 0$) as water pressure approaches ice overburden pressure. At this point, friction with the bed plummets and ice sliding velocity u_s becomes large. The opposite occurs if an efficient drainage system exists: P_w decreases as water drains, resulting in increased effective pressure (N) and frictional stress, and decreased sliding velocity u_s (e.g., Cuffey & Paterson, 2010; Schoof, 2005, 2010). Subglacial drainage efficiency is therefore a key modifier of glacial velocity and erosion.

1.1.1 Ice dynamics

The driving stress (taken to be equal to the local basal drag) τ_b, effective pressure N, and sliding velocity u_s relate to each other through a sliding law of the kind (Schoof, 2005):

$$\tau_b/N = C\left(\frac{u_s/N^n}{u_s/N^n + \Lambda_o}\right)^{1/n}, \qquad (1)$$

where τ_b is the local basal drag, taken to be equal to the driving stress $\tau_b = \rho g H S$ (ρ is ice density, g is gravity, H is ice thickness, S is ice surface slope), C is the maximum up-slope bed slope, n is the ice rheology exponent (typically $n \sim 3$) Cuffey & Paterson (2010), and Λ_o is a parameter describing the geometry of the bed:

$$\Lambda_o = \frac{\lambda A}{S_b}. \qquad (2)$$

S_b is a characteristic bed slope, A is the temperature-dependent ice softness parameter, and λ is the dominant wavelength of bed roughness (Schoof, 2010). The sliding law in equation 1 departs from other empirical power laws Herman & Braun (2008) to account for the nonphysical divergence in driving stresses when $N \to 0$ (e.g., Schoof, 2005; Hutter & Hughes, 1984).

Ice sliding is considered to be the dominant mechanism leading to glacial erosion because of the frictional and abrasive action with the substrate, although other mechanisms also participate (e.g., Alley et al., 2019; Egholm et al., 2012). Erosion rates ϵ are empirically described as depending on sliding velocity through a power-law:

$$\epsilon = K_g u_s^l, \tag{3}$$

with ϵ the erosion rate, K_g a glacial erodibility constant, and l an exponent varying between 1 and 2 (e.g., Egholm et al., 2012; Herman & Braun, 2008).

1.2 Glacial drainage

Glacial drainage modulates the ice-bed frictional stresses through the effective pressure N, and thus is a key component of glacial dynamics. Two types of drainage exist: distributed (inefficient) and channelized (efficient) (e.g., Cuffey & Paterson, 2010; Schoof, 2010; Weertman, 1972; Röthlisberger, 1972; Nye, 1976; Kamb, 1970). Distributed drainage consists of poorly connected pockets of water (cavities) that form when ice slides over bed protrusions (figure 1d and 1e). Basal meltwater moves inefficiently between cavities, increasing water pressure P_w and accelerating ice sliding through the drop in frictional stress caused by $N \to 0$ (e.g., Schoof, 2005, 2010; Gagliardini et al., 2007; Weertman, 1972). Large portions of continental Quaternary ice sheets operated in this drainage regime (e.g., A. Dyke et al., 1982; Charbit et al., 2002; Anderson et al., 2002; Johnson & Fastook, 2002; Cuffey & Paterson, 2010). These landscapes record significant sliding and associated high erosion (equation 3). Common associated landforms are striae, glacial grooves, drumlin and ribbed moraine fields, and poorly connected water pockets (figure 1d2).

In contrast, channelized drainage consists of channel networks that form well-connected drainage pathways, delivering water from the ice-bed interface to the ice margin (figures 1a and b). Water in subglacial channels flows at high discharges, following gradients in water head and effective pressure (e.g., Schoof, 2010; Nye, 1976; Hewitt, 2011). Water pressure P_w drops in the channels and in their vicinity, yielding an increase in ice-bed frictional stresses that inhibits basal sliding. Channelized water becomes the main erosional mechanism, incising channels and tunnel valleys in bedrock (figure 1d1), in sedimentary 'canals', with eskers and ice marginal deltas where sediment is deposited (e.g., Sugden et al., 1991; Walder & Fowler, 1994; Ng, 1998; Greenwood et al., 2007; Kehew et al., 2012; Storrar et al., 2014; Grau Galofre et al., 2018). Landscapes where these landforms dominate are comparatively rare, with examples in the Canadian Arctic, Antarctica, and northern Scandinavia (e.g., A. Dyke, 1999; Sugden et al., 1991; Greenwood et al., 2007; Storrar et al., 2014; Grau Galofre et al., 2018) (figure 1d).

The dominant glacial drainage mode (channel or cavity) is set by the fastest growing subglacial conduit, which follows a competition-based model of the type Schoof (2010):

$$\frac{\partial X_s}{\partial t} = c_1 Q \Psi + u_s h - c_2 N^n X_s. \tag{4}$$

A subglacial conduit cross-section grows or shrinks ($\partial X_s/\partial t$) either through the growth of a channel ($c_1 Q\Psi$) or a cavity ($u_s h$), and its closure rate ($c_2 N^n X_s$) (supplement). Subglacial channel cross-sections grow through turbulent wall melting (discharge Q times hydraulic pressure gradient Ψ), whereas cavity cross-sections grow through the sliding of ice (u_s) over bed protrusions of size h. In turn, conduits close due to ice deformation N^n at a rate proportional to the conduit cross-section X_s. The constants c_1, c_2, and c_3 are defined below. The hydraulic gradient Ψ is given by the downslope component of weight and the water pressure gradient along the conduit, and it is linked to discharge through Darcy-Weisbach's equation:

$$\Psi = \rho_w g S_t - \nabla P_w, \quad \Psi = \left(\frac{Q}{c_3 X_s^{5/4}} \right)^2 \tag{5}$$

The values of the constants in equation 4 are:

$$c_1 = \frac{1}{\rho L}; \;\; c_2 = 2An^{-n}; \;\; c_3 = 2^{1/4}\frac{\sqrt{\pi+2}}{\pi^{1/4}\sqrt{\rho_w f}}. \tag{6}$$

The transition between cavities and channels occurs at a critical discharge Q_c, defined when the cavity and channel contributions to conduit opening are equal in balancing creep closure, in steady-state (Schoof, 2010).

$$Q_c = \frac{4u_s h}{c_1(\alpha-1)\Psi}. \tag{7}$$

Ice drainage is driven by subglacial channels above Q_c, and by sliding over protrusions below Q_c (figure 1) (Schoof, 2010).

2 Sliding velocity and glacial drainage on Mars

We use equations 1 and 4 to interrogate the feedback between subglacial drainage mode and ice sliding velocity on Mars. We use the ancient southern circumpolar ice sheet as a case study (e.g., Fastook et al., 2012; Kress & Head, 2015; Butcher et al., 2016; Scanlon et al., 2018), and compare its theoretical behavior to a hypothetical ice sheet of identical thickness and geometry on Earth. Our choice of parameters (table 1, sensitivity analysis in supplement) is informed from existing work. The implications of our results easily translate to other glacial bodies, including a possible Late Noachian Icy Highlands ice sheet (e.g., Fastook & Head, 2015; Wordsworth et al., 2015).

Our work aims to isolate how gravity affects glacial hydrology, but mass balance, thermophysics, and ice deformation are important differences between terrestrial and martian ice sheets that must also be considered (e.g., Cuffey & Paterson, 2010). Considering similarly massed martian and terrestrial ice sheets, reduced driving stresses on Mars would lead to thicker, narrower ice sheets with steeper margins, enhancing mechanisms of marginal mass waste (e.g., calving). Early Mars glacial mass balance may have been similar to Earth's (e.g., Wordsworth et al., 2015; Wordsworth, 2016), but Mars' considerable elevations and lower atmospheric pressures likely favored sublimation, potentially developing a second equilibrium line altitude on glacial bodies (Fastook et al., 2008). Ice thermophysics also differed: basal heat flux is controlled by early geothermal flow, surface heat loss is controlled by ancient surface temperature conditions, and ice temperature is affected by insulation (i.e., ice thickness and dust content) and ice internal friction. The supplement analyses each of these factors, but a complete model coupling ice sheet dynamics, early Mars climate, and geothermal heat fluxes is beyond the scope of this study.

2.1 Contributions to glacial drainage evolution and drainage stability

Figure 2 illustrates the results of independently evaluating the contributions of channel enlarging by melt, cavity opening by sliding, and ice creep conduit closure to the evolution of conduit cross-section (equation 4), for small (panels a,c,e) and large (b,d,f) discharges, as given in table 1. In panels c - f we show the individual contributions to conduit opening from channels and sliding over cavities for Mars (center) and Earth (bottom panels). The dashed curve results from adding both opening contributions, whereas the black curves show closure rates. When the combined rate of conduit opening equals the cavity opening rate, cavities govern subglacial drainage, whereas channels dominate when wall melt rate equals the combined opening rate. Cross-sections from which channels (Ch) or cavities (Cv) start to dominate the drainage are marked with left or right-pointing arrows.

Panels (a) and (b) show the closure and combined opening rates on Earth and Mars. Where the sum of opening rates (dashed lines) balances the closure rates the subglacial

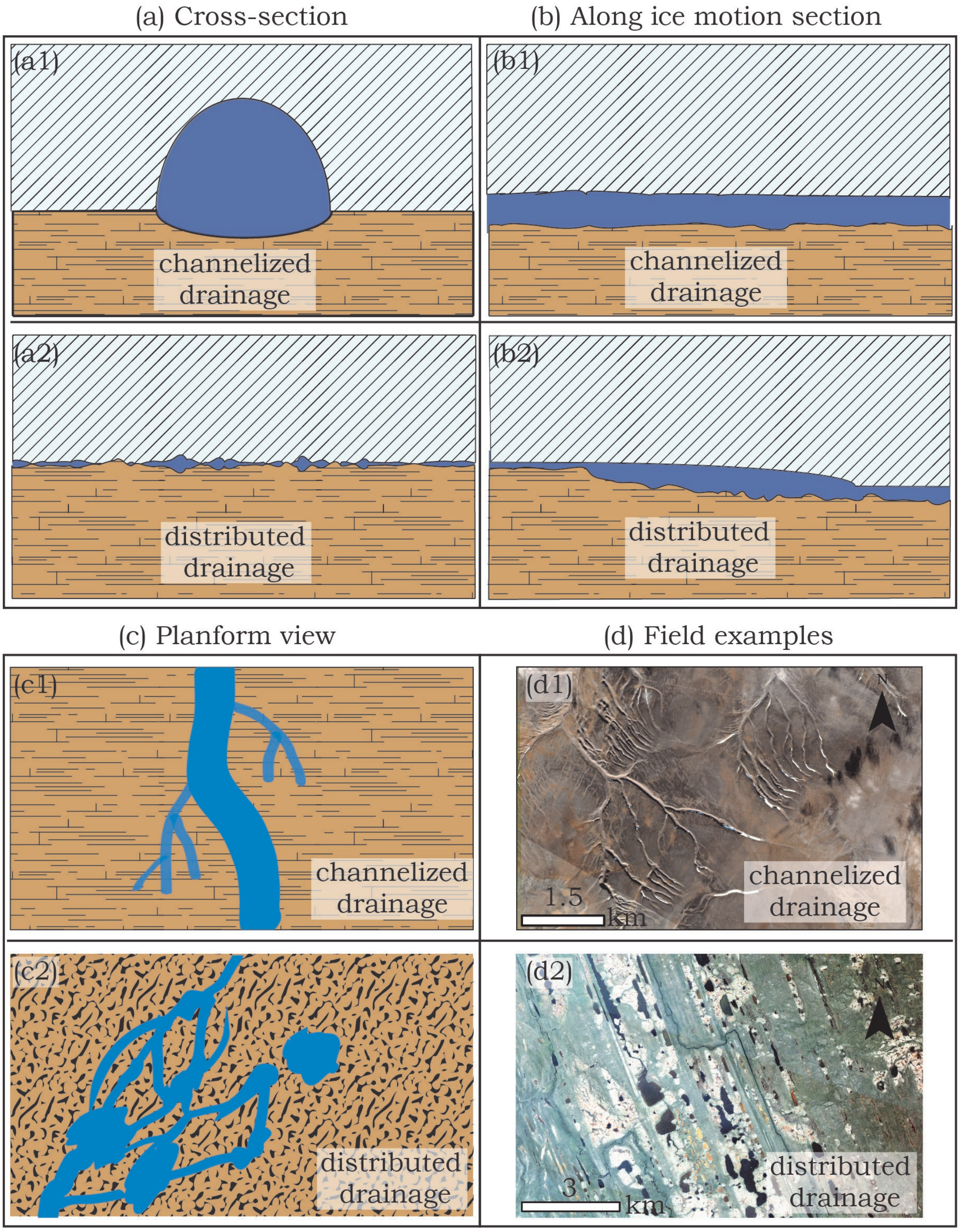

Figure 1. The drainage of wet-based ice sheets. Panels a-d show different schematic views of the subglacial drainage system (channelized or distributed). Panel (d) shows PlanetScope images of Devon Island, 75.29°N, 89.14°W (upper), and the Northwest Territories 63.67°N, 120.69°W (lower) (image IDs 805d9224-0afc-4def-8b5d-0e90aadbf1e6 and 04001a01-ffa8-46f8-9188-d77307d1c61e, Planet Team (2017). Planet Application Program Interface: In Space for Life on Earth. San Francisco, CA.).

Table 1. Parameters used to produce figure results, unless otherwise stated.

variable	description	value	units	references
g_E	Earth gravity	9.81	m/s^2	
g_M	Mars gravity	3.71	m/s^2	
ρ	ice density	917	kg/m^3	
ρ_w	water density	1000	kg/m^3	
h	Kamb step	0.1	m	Schoof (2010)
H	ice thickness	1500	m	Scanlon et al. (2018)
S	slope	0.002	ND$^{(*)}$	Scanlon et al. (2018)
T	ice temperature	270	K	
τ_γ	ice yield stress	100000	Pa	Cuffey & Paterson (2010)
Q_s	Small discharge	50	m^3/s	Scanlon et al. (2018)
Q_p	Peak discharge	30,000	m^3/s	Ng et al. (2007)
X_{ss}	Small cross-section	5	m^2	Butcher et al. (2016)
X_{sp}	Peak cross-section	350,000	m^2	Butcher et al. (2016)
n	Glen's exponent	3	ND*	Cuffey & Paterson (2010)

$^{(*)}$ND: Non-dimensional

drainage is in steady-state. There are two points where this occurs Schoof (2010): the cavity equilibrium (Eq.1, red arrow for Mars, blue for Earth), and the channel equilibrium (Eq.2).

Figure 2 shows steady-state subglacial drainage configurations at fixed N and Ψ, and highlights three main results: (1) Subglacial channels dominate the steady-state glacial hydrology at smaller cross-sections on Mars compared to Earth, becoming the main contribution to subglacial conduit opening with cross-sections up to three orders of magnitude smaller (c and d vs. e and f). Similarly, a channelized steady-state drainage configuration is achieved at smaller cross-sections for Mars than on Earth (a).

(2) Subglacial conduits are more resilient on Mars compared to Earth. Conduit closure rates on Mars are up to an order of magnitude lower due to the lower gravity, although this difference decreases when peak discharge values are considered (figure 2a and d, compare black lines). Rates of cavity growth are also lower on Mars due to the direct effect of gravity on sliding velocity through the basal drag in equation 1, implying a large conduit size difference between steady-state configurations on Earth and Mars (a, b).

(3) The dominant character of channelized over distributed drainage on Mars is consistent across a wide range of meltwater discharge values (a-c and d-e panels), from small ($Q \sim 50$ m^3/s) to peak estimated Dorsa Argentea discharge values ($Q \sim 30{,}000$ m^3/s) (Scanlon et al., 2018). Note that for Dorsa Argentea peak discharge values no subglacial drainage equilibrium is achieved under terrestrial conditions (b). Instead, channel growth displays runaway outburst (jökulhlaup) behavior (Schoof, 2010).

The implications of figure 2 are that subglacial channels should dominate the steady-state drainage configuration of Mars' wet-based ice sheets for a wide range of discharges, achieving steady conditions at lower cross-section values compared to Earth (Eq.2 in panels a and b). Slower channel closure rates (c and d) allow for stability of this drainage system over longer timescales than on Earth.

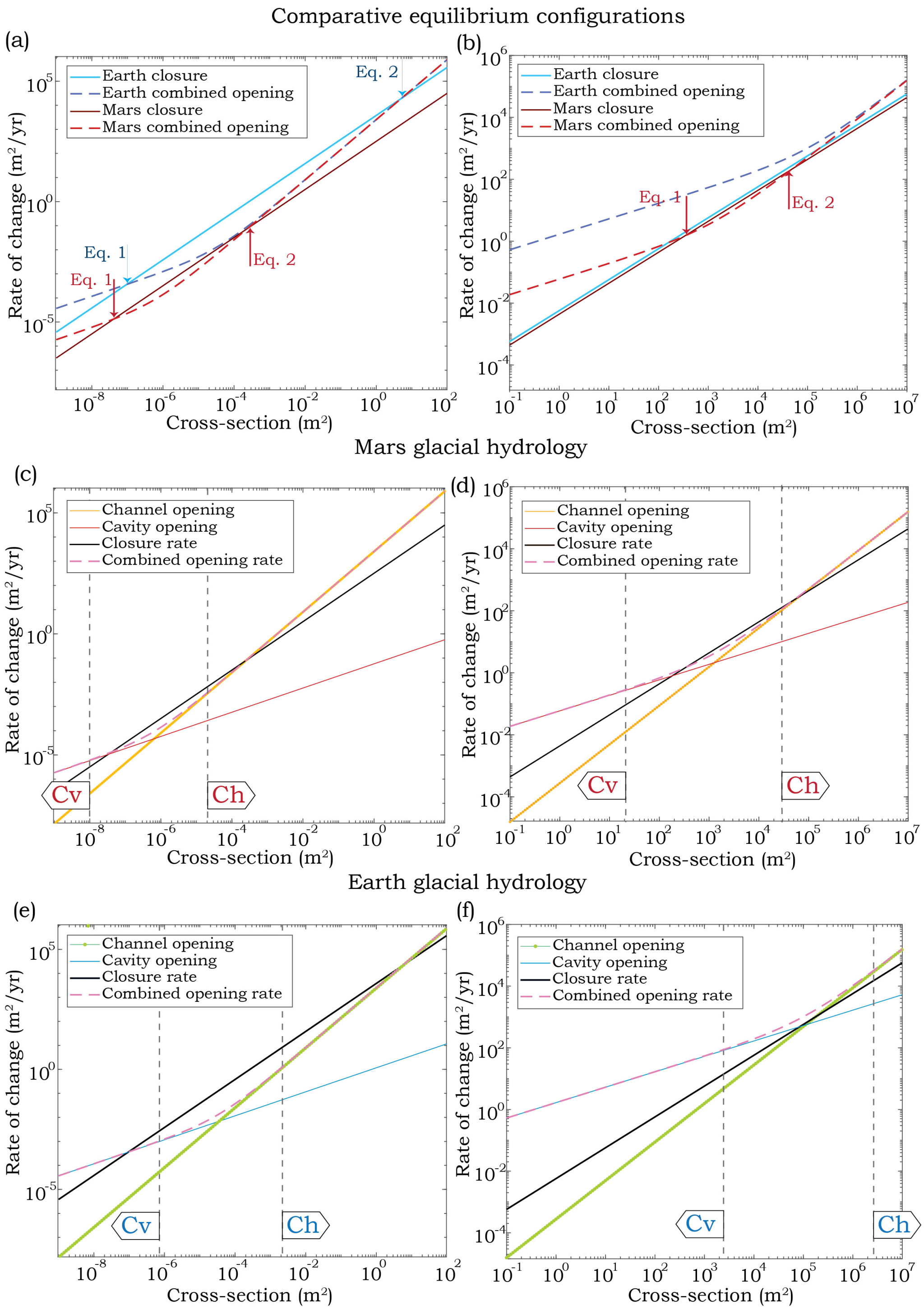

Figure 2. Rates of steady-state subglacial channel and cavity closure on Earth and Mars: y-axis is rate of cross-section change (m^2/yr) and x-axis cross-section (m^2). Panels show the results of applying equation 4 with parameters from table 1. Left side shows low discharge conditions (50 m^3/s), and right side shows peak discharge conditions (30,000 m^3/s). Steady-states, the balance of closure and combined opening rates, are shown for Earth and Mars in panels (a) and (b): Eq.1 arrows designate equilibrium drainage by cavities, whereas channels set the equilibrium indicated by Eq.2 arrows. Center and bottom panels show individual components in equation 4 for Mars (c and d) and Earth (e and f): channel and cavity opening rates, combined channel and cavity opening rates, and rate of conduit closure. 'Ch' and 'Cv' arrows mark the cross-sectional areas where channels or cavities dominate, respectively.

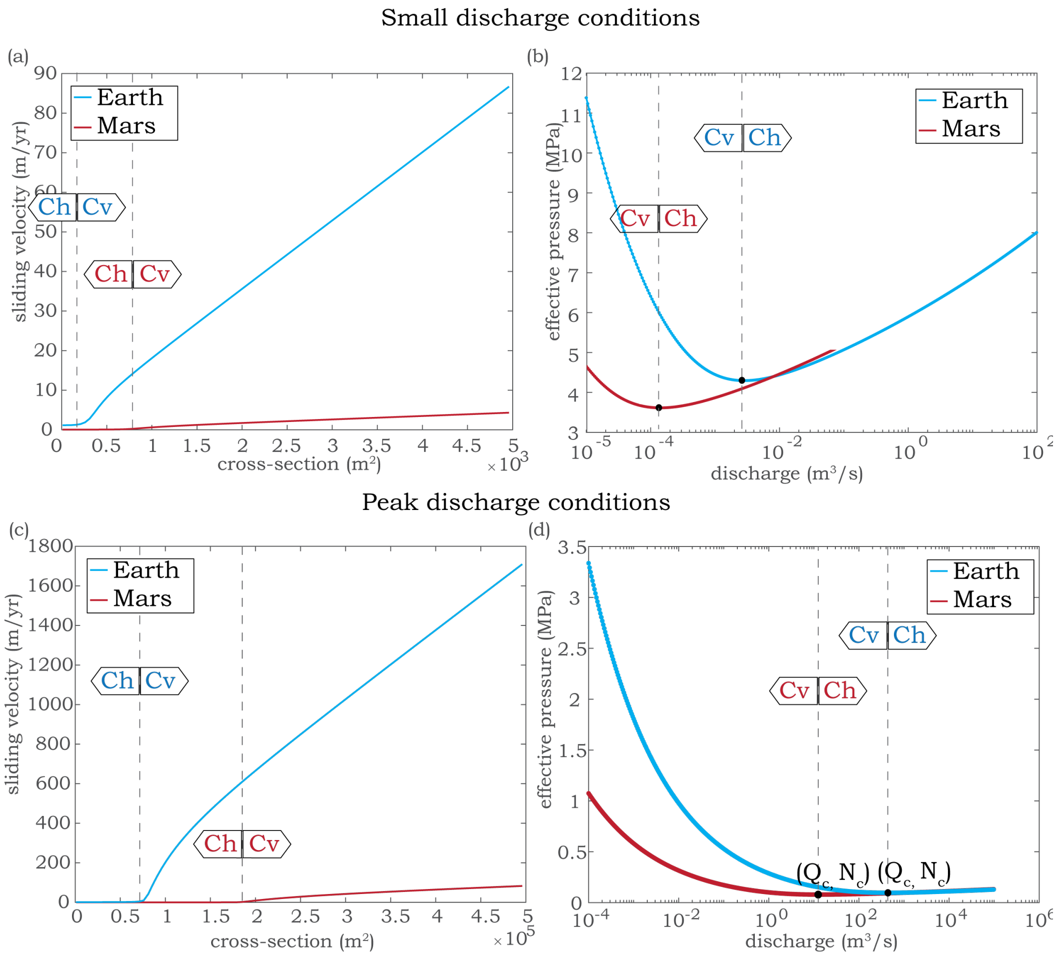

Figure 3. Left panels: Sliding velocity on Earth (blue lines) and Mars (red lines) as a function of conduit cross-section (sum of all conduit sections required to transport the given discharge) at small (a) and peak discharge conditions (c). Dashed lines indicate the drainage transition from channels (Ch) to cavities (Cv) and the associated increase in u_s. Right panels: Effective pressure N as a function of discharge Q for Mars (red lines) and Earth (blue lines), showing the critical discharge (equation 7) at which the transition from cavities (Cv) to channels (Ch) occurs. Panel (b) shows small discharge conditions, and panel (d) shows peak discharge (see table 1).

2.2 The sliding velocity of wet-based glaciers on Mars

The feedback defined by equations 1 and 4 implies that the drainage regime is a key modifier of sliding velocity through the effective pressure N. We interrogate this relationship in figure 3 and show the effects of introducing glacial hydrology to the estimation of ice sliding velocity on Mars.

We calculate the sliding velocity considering the coupling with the subglacial drainage system in equation 4. Whereas gravity already produces around a factor of six difference in the magnitude of the sliding velocity for ice masses on Earth vs. Mars before accounting for hydrology, after introducing the effects of the drainage regime in regulating glacial hydrology, the difference increases to at least a factor of 20. Panels (b) and

(d) show how the switch between distributed and channelized drainage occurs at lower discharges on Mars compared to Earth. For similar ice sheet geometries, the critical discharge for channel opening is 1-2 orders of magnitude smaller on Mars than on Earth. Because the discharge required to open and maintain a subglacial channel in equilibrium on Mars is much lower than on Earth, channelization would develop more easily and play a bigger role in the drainage of ice sheets on Mars.

3 Discussion

3.1 The resilience of the Martian subglacial drainage system

The results presented in figures 2 and 3 show that subglacial conduits on Mars close at rates slower than Earth, and that the critical discharges to keep channels open are up to two orders of magnitude smaller. Another aspect of interest is the resilience of the subglacial system to closure. In terrestrial ice sheets such as Greenland, subglacial channel collapse seasonally owing to low winter discharges, resulting in ice sheet acceleration in the early summer months when an increase in melt supply is accommodated by cavity development and fast sliding (Schoof, 2010). On Mars, slower closure rates, smaller critical discharges for channelization onset, and potentially colder ice conditions all combine to increase the stability of subglacial channels, possibly making them a stable, perennial feature of the glacial hydrological system. Equation 3.1 establishes the timescale of channel closure (supplement), from an initial cross-section X_{so} until the cross-section associated with a critical discharge X_{sf}:

$$\Delta t = \frac{2}{7c_2N^n} \ln \left(\frac{c_2N^nX_{sf}^{7/2} - c_1/c_3^2Q_c^3}{c_2N^nX_{so}^{7/2} - c_1/c_3^2Q_c^3} \right). \tag{8}$$

When Δt is larger than the duration of the winter season, Martian subglacial channels become permanent and seasonal sliding episodes are not to be expected (supplement).

3.2 The diagnostic landforms of Martian wet-based ice sheets

Considering equation 3, which describes glacial erosion by sliding, and taking the difference between terrestrial and Martian sliding rates to be a factor of 20 (figure 3), erosion rates on Mars should be between a factor of 20-400 slower than Earth, for equivalent values of the exponent l and erodibility K_g. Glacial erosion rates by terrestrial ice masses are typically between 0.1-10 mm/yr, with temperate and steep glaciers recording rates in excess of 10 mm/yr (e.g., Cuffey & Paterson, 2010; Kargel & Strom, 1992; Bernhardt et al., 2013). Martian wet-based ice sheets would thus erode on the order of $10^{-3} - 10^{-1}$ mm/yr by sliding, implying that 100 m of erosion would occur on scales of 1 Myr. Two other factors could then further hinder the development of lineated landforms (grooves, drumlines, etc.) on Mars. First, large variability in orbital parameters occurs on Mars on short timescales. For example, within the last 1 Myr, obliquity varied 20°, eccentricity varied 0.08, and insolation varied 250 W/m^2 at the north pole (Laskar et al., 2004). Whereas orbital parameters for early Mars are unclear because projections become chaotic after 40 Myr (Laskar et al., 2004), significant changes in ice distribution and stability could have occurred within the 1 Myr timescale required to produce typical lineated features, consistent with the apparent lack of glacial sliding record.

According to our results, glacial sliding on Mars could still occur in areas where the driving stress τ_b is high enough to compensate for the lower gravity (equation 1). This limits the spatial distribution of sliding landscapes to steep slopes, including crater walls or escarpments, coherently with the limited reports of the distribution of landforms possibly associated with glacial sliding on Mars, such as the southern rim of the Argyre basin (e.g., Bernhardt et al., 2013). In areas with gentler slopes, subglacial channels and/or eskers can be found accompanied by limited or no evidence of glacial sliding, including the interior of the Argyre impact structure, the Dorsa Argentea Formation, or the mid-latitudes (e.g., Fastook et al., 2012; Butcher et al., 2016; Head & Pratt, 2001; Grau Galofre, Jellinek, & Osinski, 2020; Hobley et al., 2014; Gallagher & Balme, 2015; Butcher et al., 2020).

3.3 Valley networks and ancient ice sheets

According to our results, the main fingerprints of Martian wet-based glaciation are expected to be subglacial channels and their depositional features, eskers and fans. This has implications for the origin of some valley networks as well as younger valleys on Mars (Hynek et al., 2010; Grau Galofre, Jellinek, & Osinski, 2020; Grau Galofre et al., 2018; Lee & Rice Jr, 1999; Gulick, 2001). Indeed, the particular morphology of subglacial channels may explain many of the puzzling characteristics of a large suite of Martian valleys. These include the lack of intervalley incision, the presence of longitudinal profile undulations, the presence of inverted ridges inside a number of valleys, the presence of many hanging tributary valleys, anastomosing patterns, large first order tributaries, etc. (e.g., Hynek et al., 2010; Grau Galofre, Jellinek, & Osinski, 2020; Grau Galofre et al., 2018; Lee & Rice Jr, 1999; Gulick, 2001). This type of landscape find terrestrial analogies in the high Arctic, where the retreat of thin, cold polar caps has exposed the remains of the drainage system with little evidence for glacial scouring.

4 Conclusions

In this manuscript we argue that the overall lack of landforms on Mars that on Earth are indicative of wet-based glaciation by glacial sliding, including lineal scouring at different scales, is a natural consequence of the coupled dynamics of sliding and subglacial drainage operating under martian gravity. To proceed, we adapt the terrestrial glacial hydrology framework to the surface conditions of Mars to interrogate how gravity affects the feedback linking glacial sliding velocity and subglacial drainage system. Our results show: (1) that subglacial channels establish the dominant drainage style under wet-based ice sheets on Mars; (2) that contrary to Earth, subglacial Martian channels open at small discharges and remain open for longer time spans; and (3) that as a result, sliding rates drop on Mars by a factor of 20 when compared to Earth. Our modeling results and predictions support the paradigm that glacial sliding would have been inhibited on Mars, and therefore characteristic wet-based glacial scouring landforms should be localized to regions of high shear stress (steep slopes). Instead, the fingerprints of wet-based glaciation on Mars should be subglacial channel networks and eskers, expressed by an analogue landscape in Devon Island (Nunavut, Canada), with implications for the search for ancient Martian glaciation, the origin of the valley networks, and the climate record preserved in martian landforms.

Acknowledgments
The authors would like to thank Professors C. Schoof and G. Clarke, as well as the Christensen, Whipple-Heimsath, and Conway research groups for insightful discussions. This project has received funding from the European Union's Horizon 2020 research and innovation programme under the Marie Skłodowska-Curie grant agreement MGFR 101027900 and from the School of Earth and Space Exploration (ASU) through the Exploration Fellowship. The authors declare no conflicts of interest.

Data statement Image data was provided through Planet's education and research program. Model description and parameters are available in table 1 and supplementary information, all other data is in Schoof, 2010, Scanlon et al., 2018, Cuffey and Paterson, 2010, Ng et al., 2007, and Butcher et al., 2016.

References

Alley, R., Cuffey, K., & Zoet, L. (2019). Glacial erosion: status and outlook. *Annals of Glaciology*, *60*(80), 1–13.

Anderson, J. B., Shipp, S. S., Lowe, A. L., Wellner, J. S., & Mosola, A. B. (2002). The Antarctic Ice Sheet during the Last Glacial Maximum and its subsequent retreat history: a review. *Quaternary Science Reviews*, *21*(1-3), 49–70.

Bernhardt, H., Hiesinger, H., Reiss, D., Ivanov, M., & Erkeling, G. (2013). Putative eskers and new insights into glacio-fluvial depositional settings in southern Argyre Planitia, Mars. *Planetary and Space Science*, *85*, 261–278.

Bernhardt, H., Reiss, D., Ivanov, M., Hauber, E., Hiesinger, H., Clark, J., & Orosei, R. (2019). The banded terrain on northwestern Hellas Planitia: New observations and insights into its possible formation. *Icarus*, *321*, 171–188.

Boulton, G., Hagdorn, M., Maillot, P., & Zatsepin, S. (2009). Drainage beneath ice sheets: groundwater–channel coupling, and the origin of esker systems from former ice sheets. *Quaternary Science Reviews*, *28*(7-8), 621–638.

Butcher, F. E., Balme, M. R., Conway, S. J., Gallagher, C., Arnold, N. S., Storrar, R. D., ... Hagermann, A. (2020). Morphometry of a glacier-linked esker in NW Tempe Terra, Mars, and implications for sediment-discharge dynamics of subglacial drainage. *Earth and Planetary Science Letters*, *542*, 116325.

Butcher, F. E., Balme, M. R., Gallagher, C., Arnold, N. S., Conway, S. J., Hagermann, A., & Lewis, S. R. (2017). Recent basal melting of a mid-latitude glacier on Mars. *Journal of Geophysical Research: Planets*, *122*(12), 2445–2468.

Butcher, F. E., Conway, S. J., & Arnold, N. S. (2016). Are the Dorsa Argentea on Mars eskers? *Icarus*, *275*, 65–84.

Byrne, S. (2009). The polar deposits of Mars. *Annual Review of Earth and Planetary Sciences*, *37*.

Carr, M., & Head, J. (2015). Martian surface/near-surface water inventory: Sources, sinks, and changes with time. *Geophysical Research Letters*, *42*(3), 726–732.

Charbit, S., Ritz, C., & Ramstein, G. (2002). Simulations of Northern Hemisphere ice-sheet retreat: sensitivity to physical mechanisms involved during the Last Deglaciation. *Quaternary Science Reviews*, *21*(1-3), 243–265.

Craddock, R. A., & Howard, A. D. (2002). The case for rainfall on a warm, wet early Mars. *Journal of Geophysical Research: Planets*, *107*(E11).

Cuffey, K. M., & Paterson, W. S. B. (2010). *The physics of glaciers.* Amsterdam: Academic Press.

Dyke, A. (1999). Last glacial maximum and deglaciation of Devon Island, Arctic Canada: support for an Innuitian ice sheet. *Quaternary Science Reviews*, *18*(3), 393–420.

Dyke, A., Dredge, L., & Vincent, J.-S. (1982). Configuration and dynamics of the Laurentide Ice Sheet during the Late Wisconsin maximum. *Géographie physique et Quaternaire*, *36*(1-2), 5–14.

Dyke, A. S. (1993). Landscapes of cold-centred Late Wisconsinan ice caps, Arctic Canada. *Progress in Physical Geography*, *17*(2), 223–247.

Egholm, D., Pedersen, V. K., Knudsen, M. F., & Larsen, N. K. (2012). Coupling the flow of ice, water, and sediment in a glacial landscape evolution model. *Geomorphology*, *141*, 47–66.

Fastook, J. L., & Head, J. W. (2015). Glaciation in the Late Noachian Icy Highlands: Ice accumulation, distribution, flow rates, basal melting, and top-down melting rates and patterns. *Planetary and Space Science*, *106*, 82–98.

Fastook, J. L., Head, J. W., Marchant, D. R., & Forget, F. (2008). Tropical mountain glaciers on Mars: Altitude-dependence of ice accumulation, accumulation conditions, formation times, glacier dynamics, and implications for planetary spin-axis/orbital history. *Icarus*, *198*(2), 305–317.

Fastook, J. L., Head, J. W., Marchant, D. R., Forget, F., & Madeleine, J.-B. (2012). Early Mars climate near the Noachian–Hesperian boundary: Independent evidence for cold conditions from basal melting of the south polar ice sheet (Dorsa Argentea Formation) and implications for valley network formation. *Icarus*, *219*(1), 25–40.

Gagliardini, O., Cohen, D., Råback, P., & Zwinger, T. (2007). Finite-element modeling of subglacial cavities and related friction law. *Journal of Geophysical Research: Earth Surface*, *112*(F2).

Gallagher, C., & Balme, M. (2015). Eskers in a complete, wet-based glacial system in the Phlegra Montes region, Mars. *Earth and Planetary Science Letters*, *431*, 96–109.

Glen, J. (1958). The flow law of ice: A discussion of the assumptions made in glacier theory, their experimental foundations and consequences. *IASH Publ*, *47*, 171–183.

Grau Galofre, A., Jellinek, A. M., Osinski, G., Zanetti, M., & Kukko, A. (2018). Subglacial drainage patterns of Devon Island, Canada: Detailed comparison of river and subglacial channels. *The Cryosphere*, *12*, 1461–1478.

Grau Galofre, A., Jellinek, A. M., & Osinski, G. R. (2020). Valley formation on early Mars by subglacial and fluvial erosion. *Nature Geoscience*, *13*(10), 663–668.

Grau Galofre, A., Osinski, G., Jellinek, A., & Chartrand, S. (2020). The Canadian Arctic Archipelago as a Mars Wet-Based Glacial Analogue Site. *LPI*(2326), 2747.

Greenwood, S. L., Clark, C. D., & Hughes, A. L. (2007). Formalising an inversion methodology for reconstructing ice-sheet retreat patterns from meltwater channels: application to the British Ice Sheet. *Journal of Quaternary Science*, *22*(6), 637–645.

Gulick, V. C. (2001). Origin of the valley networks on Mars: A hydrological perspective. *Geomorphology*, *37*(3-4), 241–268.

Head, J. W., & Pratt, S. (2001). Extensive Hesperian-aged south polar ice sheet on Mars: Evidence for massive melting and retreat, and lateral flow and ponding of meltwater. *Journal of Geophysical Research: Planets*, *106*(E6), 12275–12299.

Herman, F., & Braun, J. (2008). Evolution of the glacial landscape of the Southern Alps of New Zealand: Insights from a glacial erosion model. *Journal of Geophysical Research: Earth Surface*, *113*(F2).

Hewitt, I. J. (2011). Modelling distributed and channelized subglacial drainage: the spacing of channels. *Journal of Glaciology*, *57*(202), 302–314.

Hobley, D. E., Howard, A. D., & Moore, J. M. (2014). Fresh shallow valleys in the Martian midlatitudes as features formed by meltwater flow beneath ice. *Journal of Geophysical Research: Planets*, *119*(1), 128–153.

Howard, A. (1981). Etched plains and braided ridges of the south polar region of Mars: Features produced by basal melting of ground ice? *Reports of Planetary Geology Program*, 286–288.

Howard, A. D., Moore, J. M., & Irwin, R. P. (2005). An intense terminal epoch of widespread fluvial activity on early Mars: 1. Valley network incision and associated deposits. *Journal of Geophysical Research: Planets*, *110*(E12).

Hubbard, B., Souness, C., & Brough, S. (2014). Glacier-like forms on Mars. *The Cryosphere*, *8*(6), 2047–2061.

Hutter, K., & Hughes, T. (1984). Theoretical glaciology. *Journal of Applied Mechanics*, *51*(4), 948.

Hynek, B. M., Beach, M., & Hoke, M. R. (2010). Updated global map of Martian valley networks and implications for climate and hydrologic processes. *Journal of Geophysical Research: Planets*, *115*(E9).

Johnson, J., & Fastook, J. L. (2002). Northern Hemisphere glaciation and its sensitivity to basal melt water. *Quaternary International*, *95*, 65–74.

Kamb, B. (1970). Sliding motion of glaciers: theory and observation. *Reviews of*

Geophysics, *8*(4), 673–728.

Kargel, J. S., Baker, V. R., Begét, J. E., Lockwood, J. F., Péwé, T. L., Shaw, J. S., & Strom, R. G. (1995). Evidence of ancient continental glaciation in the Martian northern plains. *Journal of Geophysical Research: Planets*, *100*(E3), 5351–5368.

Kargel, J. S., & Strom, R. G. (1992). Ancient glaciation on Mars. *Geology*, *20*(1), 3–7.

Kehew, A. E., Piotrowski, J. A., & Jørgensen, F. (2012). Tunnel valleys: Concepts and controversies—A review. *Earth-Science Reviews*, *113*(1), 33–58.

Kress, A. M., & Head, J. W. (2015). Late Noachian and early Hesperian ridge systems in the south circumpolar Dorsa Argentea Formation, Mars: Evidence for two stages of melting of an extensive late Noachian ice sheet. *Planetary and Space Science*, *109*, 1–20.

Laskar, J., Correia, A., Gastineau, M., Joutel, F., Levrard, B., & Robutel, P. (2004). Long term evolution and chaotic diffusion of the insolation quantities of Mars. *Icarus*, *170*(2), 343–364.

Lee, P., & Rice Jr, J. W. (1999). Small Valleys Networks on Mars: The Glacial Meltwater Channel Networks of Devon Island, Nunavut Territory, Arctic Canada, as Possible Analogs. In *The fifth international conference on mars* (Vol. 20000110394).

Ng, F. S. (1998). Mathematical modelling of subglacial drainage and erosion (doctoral dissertation).

Ng, F. S., Liu, S., Mavlyudov, B., & Wang, Y. (2007). Climatic control on the peak discharge of glacier outburst floods. *Geophysical Research Letters*, *34*(21).

Nye, J. (1976). Water flow in glaciers: jökulhlaups, tunnels and veins. *Journal of Glaciology*, *17*, 181–207.

Nye, J., Durham, W., Schenk, P., & Moore, J. (2000). The instability of a south polar cap on Mars composed of carbon dioxide. *Icarus*, *144*(2), 449–455.

Röthlisberger, H. (1972). Water pressure in intra-and subglacial channels. *Journal of Glaciology*, *11*(62), 177–203.

Scanlon, K., Head, J., Fastook, J., & Wordsworth, R. (2018). The Dorsa Argentea Formation and the Noachian-Hesperian climate transition. *Icarus*, *299*, 339–363.

Schoof, C. (2005). The effect of cavitation on glacier sliding. In *Proceedings of the royal society of london a: Mathematical, physical and engineering sciences* (Vol. 461, pp. 609–627).

Schoof, C. (2010). Ice-sheet acceleration driven by melt supply variability. *Nature*, *468*(7325), 803–806.

Storrar, R. D., Stokes, C. R., & Evans, D. J. (2014). Morphometry and pattern of a large sample (¿ 20,000) of Canadian eskers and implications for subglacial drainage beneath ice sheets. *Quaternary Science Reviews*, *105*, 1–25.

Sugden, D. E., Denton, G. H., & Marchant, D. R. (1991). Subglacial meltwater channel systems and ice sheet overriding, Asgard Range, Antarctica. *Geografiska Annaler. Series A. Physical Geography*, 109–121.

Walder, J. S., & Fowler, A. (1994). Channelized subglacial drainage over a deformable bed. *Journal of Glaciology*, *40*(134), 3–15.

Weertman, J. (1972). General theory of water flow at the base of a glacier or ice sheet. *Reviews of Geophysics*, *10*(1), 287–333.

Wordsworth, R. D. (2016). The climate of early Mars. *Annual Review of Earth and Planetary Sciences*, *44*, 381–408.

Wordsworth, R. D., Kerber, L., Pierrehumbert, R. T., Forget, F., & Head, J. W. (2015). Comparison of “warm and wet” and “cold and icy” scenarios for early Mars in a 3-D climate model. *Journal of Geophysical Research: Planets*, *120*(6), 1201–1219.